Ecological Modelling 220 (2009) 2121–2136

Contents lists available at ScienceDirect

Ecological Modelling

journal homepage: www.elsevier.com/locate/ecolmodel

Optimization of ecosystem model parameters using spatio-temporal soil moisture information

Lin Zhu [a,b,d,*], Jing M. Chen [b], Qiming Qin [a], Jianping Li [c], Lianxi Wang [c]

[a] Institute of Remote Sensing and GIS, Peking University, Beijing, 100871, China
[b] Department of Geography, University of Toronto, Toronto, M5S 3G3, Canada
[c] Ningxia Key Laboratory for Meteorological Disaster Prevention and Reduction, Yinchuan, 750002, China
[d] National Satellite Meteorological Center of China Meteorological Administration, Beijing, 100081, China

ARTICLE INFO

Article history:
Received 10 December 2008
Received in revised form 21 April 2009
Accepted 24 April 2009
Available online 6 June 2009

Keywords:
Parameter optimizing
Soil moisture
Ensemble Kalman Filter
Remote sensing

ABSTRACT

Parameters in process-based terrestrial ecosystem models are often nonlinearly related to the water flux to the atmosphere, and they also change temporally and spatially. Therefore, for estimating soil moisture, process-based terrestrial ecosystem models inevitably need to specify spatially and temporally variant model parameters. This study presents a two-stage data assimilation scheme (TSDA) to spatially and temporally optimize some key parameters of an ecosystem model which are closely related to soil moisture. At the first stage, a simplified ecosystem model, namely the Boreal Ecosystem Productivity Simulator (BEPS), is used to obtain the prior estimation of daily soil moisture. After the spatial distribution of 0–10 cm surface soil moisture is derived from remote sensing, an Ensemble Kalman Filter is used to minimize the difference between the remote sensing model results, through optimizing some model parameters spatially. At the second stage, BEPS is reinitialized using the optimized parameters to provide the updated model predictions of daily soil moisture. TSDA has been applied to an arid and semi-arid area of northwest China, and the performance of the model for estimating daily 0–10 cm soil moisture after parameter optimization was validated using field measurements. Results indicate that the TSDA developed in this study is robust and efficient in both temporal and spatial model parameter optimization. After performing the optimization, the correlation (r^2) between model-predicted 0–10 cm soil moisture and field measurement increased from 0.66 to 0.75. It is demonstrated that spatial and temporal optimization of ecosystem model parameters can not only improve the model prediction of daily soil moisture but also help to understand the spatial and temporal variation of some key parameters in an ecosystem model and the corresponding ecological mechanisms controlling the variation.

1. Introduction

Soil water content is a key variable for estimating plant growth and energy exchange between the surface and the atmosphere (Gillies, 1997; Zhan et al., 2007). Accurate estimation of soil water content is especially important for regional agricultural, hydrological and meteorological research and for the understanding land surface processes (Hanson et al., 1998; Silberstein et al., 1999; Heathman et al., 2003; Eitzinger et al., 2004).

While the most direct way to determine soil water content is based on field measurements, using techniques such as the gravimetric sampling or the calibrated time-domain reflectometry (TDR) (Topp et al., 1980; Klute, 1986), it is impractical and expensive to conduct such measurements for large areas (Heathman et al., 2003; Huang et al., 2008). Compared to point-based field measurements, remote sensing techniques would be most feasible for large area applications. Indices derived from visible and near infrared bands (Zhan et al., 2007; Ghulam et al., 2007a,c), shortwave infrared bands (Ghulam et al., 2007b); thermal infrared bands (Price, 1985; Kogan, 1995; Mcvicar and Jupp, 1998; Sandholt et al., 2002) and even microwave bands (Schmugge et al., 1986; Njoku and Li, 1999) are widely used to capture spatial and temporal soil moisture variations near the surface. However, no matter which bands are used, signals from remote sensing only represent instantaneous and near surface soil moisture conditions, and they are only sensitive to soil moisture in the top few centimeters (less than 10 cm) of the soil column (Li and Islam, 2002). This limitation of remote sensing data hinders their applications in regional agricultural, hydrological and meteorological studies.

The development of modeling techniques is an attempt to estimate the vertical distribution of soil moisture that can extend the near surface information derived from remote sensing. Ecosystem models relate some key variables of the land surface in a mathematical framework (Pipunic et al., 2008) and provide a mechanistic

* Corresponding author. Tel.: +86 10 62764430.
E-mail address: hongfuqitian@pku.edu.cn (L. Zhu).

0304-3800/$ – see front matter © 2009 Elsevier B.V. All rights reserved.
doi:10.1016/j.ecolmodel.2009.04.042

description of every process which contributes to the total soil moisture variation (Liu et al., 2003; Ju et al., 2006; Walker and Langridge, 2006; Chen et al., 2007). Therefore, an ecosystem model is helpful to understand the feedback between soil and atmosphere as well as plant growth and carbon uptake (Bach and Mauser, 2003). In ecosystem models, water fluxes can be calculated for a defined period so that the temporal variation of soil moisture can be studied (Liu et al., 2003). However, the major problems of ecosystem models may include overly simplified description of the natural system, and inaccurate parameterization, both of which strongly influence the model performance at a regional scale (Zhao et al., 2005; Dorigo et al., 2007; Naud et al., 2007). In particular, parameters change temporally and spatially, while the field measurements to calibrate these parameters are not always available or very often we only have data from discrete weather stations. Errors due to poor specification of model parameters will accumulate gradually and therefore, soil moisture estimation will diverge from the true state when a model is run for a period of several days.

It has recently been suggested that soil moisture could be better estimated through assimilating various observations (e.g. fluxes from field measurements, remote sensing data) into ecosystem models to best use all sources of information (Kostov and Jackson, 1993; Moradkhani, 2008). The main objective of data assimilation is to find an optimal estimation of model state variables using observations. Therefore data assimilation can be used to bridge the gap between a remote sensing observation of the land surface and a process-based model (Bach and Mauser, 2003). Remote sensing data from moderate spatial resolution earth observation sensors, such as MODIS on board NASA Terre or Vegetation sensor on board SPOT4 and SPOT5, are promising candidates for generating data suitable for model improvement due to their high temporal resolutions and large spatial scales (Quaife et al., 2008; Pipunic et al., 2008; Huang et al., 2008).

Although data assimilation techniques provide a promising way to improve soil moisture estimation, the validity of data assimilation is strongly dependent on the quality of remote sensing information and its sampling frequency. Information from optical and thermal infrared sensors is influenced by atmospheric conditions, especially clouds, water vapor and aerosol distribution (Huang et al., 2008). Furthermore, the heterogeneity of the land surface at large spatial scales requires remote sensing signals or remote sensing land surface products to be further calibrated using field measurements. For most meteorological stations, the field measurements for soil moisture are always sampled at intervals of several days. Therefore, high quality remote sensing data at daily time steps are often limited.

Confined to the availability of high quality remote sensing observations, uncertainty in model state variables will propagate if model parameters have changed between two observations (Dorigo et al., 2007; Quaife et al., 2008). Accordingly, the model prediction error of soil moisture still accumulates during this period. Therefore, ecosystem models inevitably need parameter optimization to improve model initialization and prediction.

Combining parameter estimation with data assimilation techniques is a recent approach to achieve high model performance (Kuroda and Kishi, 2004; Moradkhani, 2004; Raupach et al., 2005; Sacks et al., 2006; Mo et al., 2008). This approach overcomes the shortcomings of traditional methods assuming time-invariant parameters (Braswell et al., 2005). Mo et al. (2008) use an Ensemble Kalman Filter (EnKF) to optimize some key parameters of the Boreal Ecosystem Productivity Simulator (BEPS) (Liu et al., 1997; Chen et al., 1999). Their study demonstrated the feasibility of retrieving the seasonal and inter-annual variation of model parameters through assimilating eddy covariance fluxes.

This study is a spatial development of Mo et al.'s (2008) method to combine both parameter estimation and data assimilation techniques to optimize some key parameters of the BEPS model and further improve surface soil moisture estimation. A two stage data assimilation scheme (TSDA) is developed to assimilate remote sensing observations into the BEPS model for parameter optimization and soil moisture estimation. The TSDA has been applied to an arid and semi-arid area in northwest China. Model performance in estimating 0–10 cm soil moisture is evaluated based on field measurements. Spatial and temporal variations of some key parameters after data assimilation and the corresponding ecological mechanisms controlling their variation are also investigated.

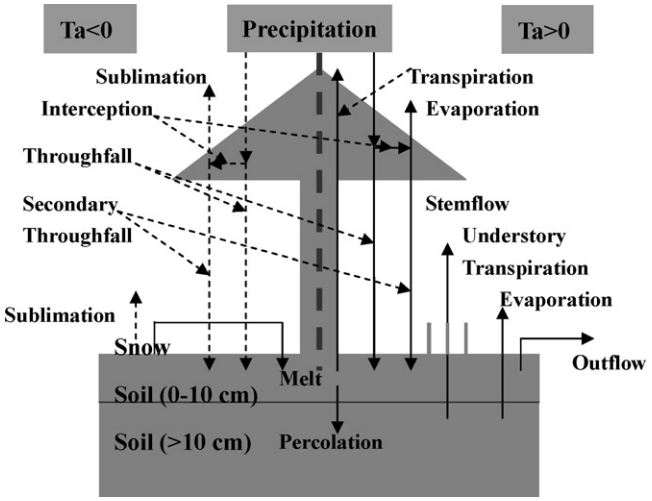

Fig. 1. Water fluxes included in BEPS based on Liu et al. (2003).

2. Methods

2.1. The ecosystem model

BEPS is a process-based ecosystem model which was originally developed for forest ecosystem carbon budget simulation. Water flux estimation is an important part of the model because of the close relationship between soil water regime and carbon uptake (Liu et al., 2003). In order to represent the importance of vegetation conditions on the water cycle, a canopy in BEPS is stratified into over-story and under-story two layers, and each layer is separated into sunlit and shaded leaf groups. Under this framework, water fluxes of all components in the hydrological cycle are captured as shown in Fig. 1.

Daily soil water balance in BEPS was calculated using a "bucket" model, in which soil water balance is calculated as:

$$\Delta W = P + S - T_0 - T_u - R_s - E_s \quad (1)$$

where ΔW is water storage change in soil; P is precipitation; T_0 is over-story transpiration; T_u is under-story transpiration; S is snow melt water; R_s is surface run-off; and E_s is evaporation from soil.

To assimilate surface soil water content derived from remote sensing, we further divide the soil profile into two layers: 0–10 cm and 10 cm to the top of saturated zone. This study focuses on simulating soil moisture in a crop area. For most crop types, it is found that the root depth is much shallower than the water table depth and the influence of the capillary rise on the root zone is small, so the saturated zone water balance and the effect of capillary rise are not considered in this study.

Water balance in the 0–10 cm (layer 1) is calculated as

$$\Delta W_{layer1} = P + S - E_{layer1} - W_p \quad (2)$$

where E_{layer1} is the total evapotranspiration in layer 1; W_p is the vertical water percolation from layer 1 to layer 2. W_p is computed

from

$$W_p = \begin{cases} P + S + \theta_{layer1} - E_{layer1} - \theta_{fc1}, & \text{if } (P + S + \theta_{layer1} - E_{layer1}) > \theta_{fc1} \\ 0, & \text{else} \end{cases} \quad (3)$$

where θ_{fc1} is the field capacity of layer 1; θ_{layer1} is water in layer 1 at last time step.

Water balance in the layer from 10 cm to the top of saturated zone (layer 2) is calculated as

$$\Delta W_{layer2} = W_p - E_{layer2} - R_{off} \quad (4)$$

where T_{layer2} is the canopy transpiration in layer 2; E_{layer2} is the total evapotranspiration in layer 2; R_{off} is the runoff water in layer 2 which is calculated as follows

$$R_{off} = \begin{cases} W_p + \theta_{layer2} - E_{layer2} - \theta_{fc2}, & \text{if } (W_p + \theta_{layer2} - E_{layer2}) > \theta_{fc2} \\ 0, & \text{else} \end{cases} \quad (5)$$

where θ_{fc2} is the field capacity of layer 2; θ_{layer2} is water in layer 2 at last time step.

In BEPS, the Penman–Monteith equation (Monteith, 1965) is used to calculate canopy transpiration in the whole soil layer. The Jarvis model (Jarvis and Morison, 1981) is used to reduce the maximum stomatal conductance by environmental conditions to the actual stomatal conductance. Leaf area index (LAI) and stomatal conductance strongly influence the calculation of total transpiration and therefore they are very sensitive to soil water calculation. Accounting for the influence of soil water content on the daily variation of stomatal conductance, the Jarvis model is further modified as a function of soil water content (Chen et al., 2005).

Furthermore, in order to separate the total evapotranspiration into layer 1 and layer 2, we need to know the vertical distribution of the root density. In this study, a root depth coefficient β (Gale and Grigal, 1987; Jackson et al., 1996) is used to compute the root vertical distribution within each soil layer.

$$f(z, \beta) = 1 - \beta^Z \quad (6)$$

where $f(z, \beta)$ describes the cumulative root fraction from the soil surface to depth z (cm). High β values indicate larger proportions of roots at a deeper soil depth, and low β values imply larger proportions of roots near the soil surface (Chen et al., 2005).

Using the root depth coefficient β, evapotranspiration rates for layer 1 and layer 2 are calculated separately as shown in Eqs. (7) and (8).

$$(T + E_s)_{layer1} = (1 - \beta^{10})(T_o + T_u + E_s) \quad (7)$$

$$(T + E_s)_{layer2} = \beta^{10}(T_o + T_u + E_s) \quad (8)$$

To summarize from Eqs. (1) to (8), *LAI*, g_{max} and β are major parameters for the calculation of water balance in BEPS. They change spatially and temporally and were previously determined from empirical data. As field measurements of these parameters for validation are not always available, the uncertainties in their initial values are considerable. Furthermore, if these three parameters are not specified temporally, errors in water balance estimation will be accumulated over the modeling period. Considering that, in BEPS, *LAI* is a model input parameter which is periodically updated from Vegetation images (Deng et al., 2006), this study focuses on optimizing g_{max} and β in BEPS using TSDA method.

The time step of BEPS is set as daily and forcing data include atmospheric variables (temperature, humidity, wind speed, precipitation, solar irradiation), *LAI* from 10 day syntheses SPOT VEGETATION images and vegetation type. The model outputs include daily soil moisture at the two layers (0–10 cm and 10 cm to the top of the saturated zone), ET, NPP, etc.

2.2. Ensemble Kalman Filter

Ensemble Kalman Filter is first developed by Evensen (1994) based on the original Kalman filter (Kalman, 1960). EnKF has gained popularity in soil moisture assimilation problems with its simple conceptual formulation and relative ease of implementation compared with the Extended Kalman Filter (EKF) (Entekhabi et al., 1994; Houser et al., 1998; Hoeben and Troch, 2000; Reichle et al., 2007).

Typically, there are two sets of dynamic ensembles in EnKF data assimilation process. One is observation ensemble (x^j_{obs}), and the other is state/parameter ensemble (x^j) (Burgers et al., 1998; Reichle et al., 2002a,b; Moradkhani, 2004). Each ensemble is generated by adding a noise with a Gaussian probability distribution to the first-guess estimate as shown in Eqs. (9) and (10)

$$x^j = x + \varepsilon^j, \quad \varepsilon^j \sim N(0, R_x), \quad j = 1, \ldots, N \quad (9)$$

$$x^j_{obs} = x_{obs} + \varepsilon^j_{obs}, \quad \varepsilon^j_{obs} \sim N(0, R_{obs}), \quad j = 1, \ldots, N \quad (10)$$

where x and x_{obs} are, respectively, the first guess of the state/parameter ensemble and the observation ensemble, which are added by a noise of ε^j and ε^j_{obs}, respectively. R_x is error covariance of states/parameters and R_{obs} is error covariance of observations. The method to determine R_x and R_{obs} are described in Sections 3.2 and 3.3, respectively. N is the ensemble size (number of realizations in each ensemble).

At time steps when the observation ensemble is available, Eq. (11) is used to modify the state/parameter forecast with the observations, to generate the best estimation of system state/parameters, which make the model output most consistent with observations.

$$x^{j+} = x^{j-} + K(x^j_{obs} - H(x^j)) \quad (11)$$

where x represents the state/parameter to be optimized; superscript '+' refer to updated quantities of state/parameters; x_{obs} is the observation; H is the observation operator which is used to make the matrix dimensions of the model state and observations comparable; $(x^j_{obs} - H(x^j))$ in Eq. (11) is called "innovation" in EnKF; K is the Kalman gain computed using the following equation

$$K = (P^- H^T)(HP^- H^T + R_{obs})^{-1} \quad (12)$$

where P^- is the priori estimate of state/parameter covariance; R_{obs} is the observation covariance. A detailed description of how to compute K can be found in Mandel (2007). Innovation $(x^j_{obs} - H(x^j))$ and Kalman gain (K) multiply together to determine the correction added to the model forecast state/parameter (Pipunic et al., 2008).

2.3. Remote sensing observation

In this study, MODIS derived soil moisture is used as spatial observations to be assimilated into BEPS. First, a water stress index-SPSI (Shortwave Infrared Perpendicular water stress Index) (Ghulam et al., 2007b) is calculated from MODIS images. Then SPSI is converted to surface soil moisture using a linear relationship between SPSI and field soil moisture measurements (as seen in Section 3.2).

SPSI is expressed as:

$$SPSI = \frac{1}{\sqrt{M^2 + 1}}(R_{SWIR} + M \times R_{NIR}) \quad (13)$$

where M is the slope of soil line in the scatter plot of near infrared (R_{NIR}) and shortwave infrared bands (R_{SWIR}).

SPSI has been demonstrated to be very sensitive to canopy water content using Landsat ETM/TM images (Ghulam et al., 2007b). For moderate resolution sensors such as MODIS, their shortwave infrared channel (1628–1652 nm) is also sensitive to water condition of the land surface because it has a higher spectral resolution

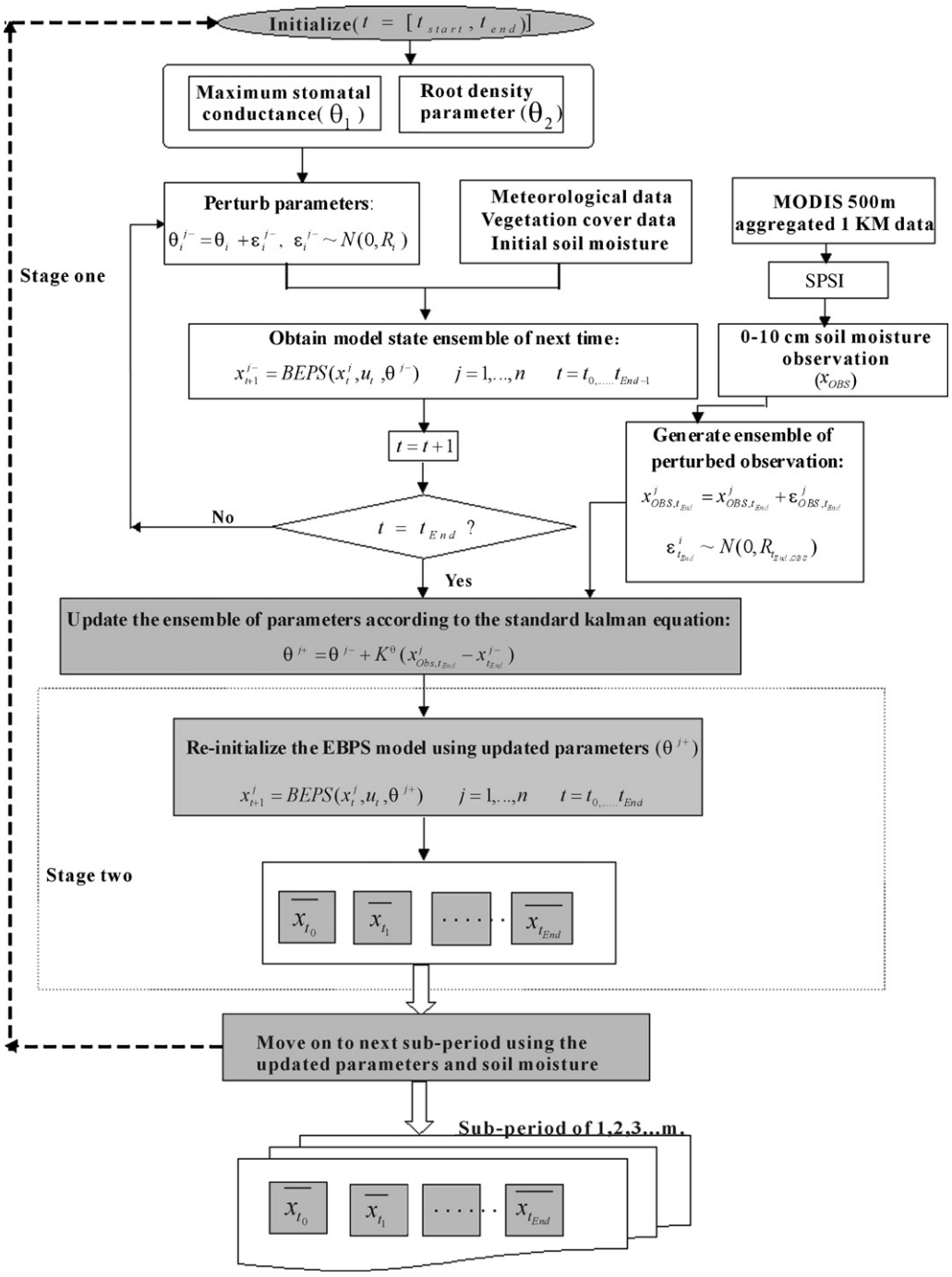

Fig. 2. Flowchart of a two-step data assimilation scheme.

which avoids the influence of water absorption from atmosphere and allows for a closer relationship between leaf water content and soil water conditions.

2.4. Data assimilation strategy

To address the issues of parameter optimization and remote sensing soil moisture data assimilation, a study period is first divided into several sub-periods according to the availability of cloud-free remote sensing observations and field measurements. For each sub-period, a two-stage data assimilation scheme (TSDA) is developed to spatially and temporally optimize some key parameters of the BEPS model (as shown in Fig. 2). At the first stage, BEPS was initialized using three parameter ensembles including *LAI*, g_{max} and β together with atmospheric forcing data, land cover data and initial soil moisture profile (as forecast, which is denoted as '−' in Fig. 2). Here, *LAI* is also perturbed as an adjustable ensemble to account for uncertainty in *LAI* input. Initial parameter ensembles (denoted as θ) are generated by adding a random noise with zero mean and parameter covariance (R_X). When remote sensing measurements are available, they are converted into the spectral index SPSI, and then SPSI is converted into 0–10 cm soil moisture estimation using a linear function. An observation ensemble is generated by adding a noise with zero mean and observation covariance (R_{obs}). Then the EnKF was used to minimize the difference between model-simulated 0–10 cm soil moisture and remotely sensed surface soil

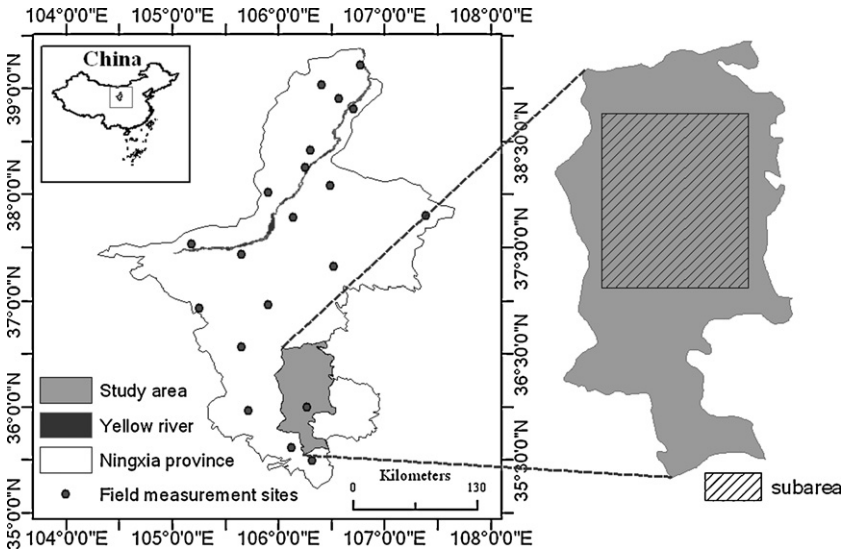

Fig. 3. The location of study area and its subarea for demonstrating the temporal and spatial variations of model parameters.

moisture. In this process, values of initial parameter ensembles are changed using the parameter-updating equation of the EnKF (Eq. (11)). At the second stage, BEPS is reinitialized using the optimized parameters to provide updated model predictions of daily soil moisture.

The updated mean values of parameters and their error covariance are further used to generate new ensembles of parameters in the next sub-period.

3. Study area and data preparation

3.1. Study area and data sources

A case study was conducted in the main drought area of Ningxia province, China. Its longitudes range from 104°10′E to 107°30′E, and latitudes range from 35°25′N to 39°25′N (Fig. 3). It is a typical arid and semi-arid region with very little precipitation (200–400 mm/a). Estimated annual potential evapotranspiration is about 2000 mm.

Guyuan city (105.96°–106.53°E, 35.56°–36.63°N) was chosen as the study area to test the data assimilation strategy. Guyuan city is located in the southern mountainous region of Ningxia. It has various vegetation types including crop, grass, and forest in addition to bare land. Crops here are mainly rain-fed. The highest daily precipitation observed is only 23.5 mm, while mean precipitation per day is 2.9 mm over the last 6 years, which led to heavy drought events almost every year, specifically in spring and summer (Ghulam et al., 2008). The study period covers a main growing season of crop from March to July 2004 and was divided into 8 sub-periods as showed in Table 1.

Daily meteorological data, including radiation, minimum and maximum temperatures, mean humidity and total precipitation of the study area, were measured by Ningxia Key Laboratory for Meteorological Disaster Prevention and Reduction of China. The land cover map was initially derived from supervised classification of TM images during the growing season (registered on August 12, 1999) and then re-sampled to 1 km resolution. LAI was derived from the 1 km resolution SPOT VEGETATION data using algorithms developed by Deng et al. (2006).

Field measurements of soil moisture and LAI were performed in collaboration with Ningxia Key Laboratory for Meteorological Disaster Prevention and Reduction (Ghulam et al., 2008). Soil moisture measurements from different soil depths of 10 cm, 20 cm, 30 cm, 40 cm, 50 cm were sampled on dates 8, 18 and 28 of every month in the study area from March to July 2004. The contemporaneous MODIS data were downloaded from NASA (http://modis–land.gsfc.nasa.gov/).

3.2. Determining the observation operator and observation error of the study area

Determining the observation operator and error is very important for the application of the assimilation scheme. The observation operator represents the H in Eq. (11), which helps convert remote sensing observations into data which are comparable to the model simulation. The observation error determines the extent to which the observation can be used to adjust the model simulation.

Field measurements of 0–10 cm soil moisture in the study area were used to validate the relationship between SPSI and 0–10 cm soil moisture at 1 km resolution. There are totally 20 sample sites in Ningxia province. To avoid the influence of irrigation on the soil moisture measurements, only 7 sample sites in the southern Ningxia province were used where no irrigation occurred. It is worth noting that, for crop areas, two or more different crops

Table 1
Division of sub-period and availability of remote sensing observations and field measurements during the whole study period (year: 2004).

Day of year	Sub-period	Clouds free remote sensing images available day (Day of year)	Field measurement available day (Day of year)
78–99	1	99	99
99–109	2	109	109
109–119	3	119	119
119–129	4	129	129
129–139	5	139	139
139–149	6	149	149
149–163	7	163	159
163–170	8	170	170

were planted in the same area in an interlaced way. So the average of soil moisture measurements of different crops around a sample site was used to represent the real 0–10 cm soil moisture at 1 km resolution.

The scatter plots between soil moisture measurements (volume percentage) and SPSI during the crop growing season of 2004 are shown in Fig. 4. It is found that SPSI derived from MODIS 1 km resolution images has a close relationship with simultaneous 0–10 cm soil moisture measurements in the field. The highest absolute value of linear correlation coefficient between soil moisture measured in the field and SPSIs is 0.98, and lowest is 0.87. The standard deviation (SD) varies between 0.010 and 0.034. The linear function between soil moisture and SPSI at each time was used to derive surface soil moisture from MODIS images, and the corresponding SD is used to account for the observation error in the EnKF.

3.3. Determining of model error

Model errors determine the uncertainty associated with the assimilated model states (Mitchell and Houtekamer, 2002; Huang

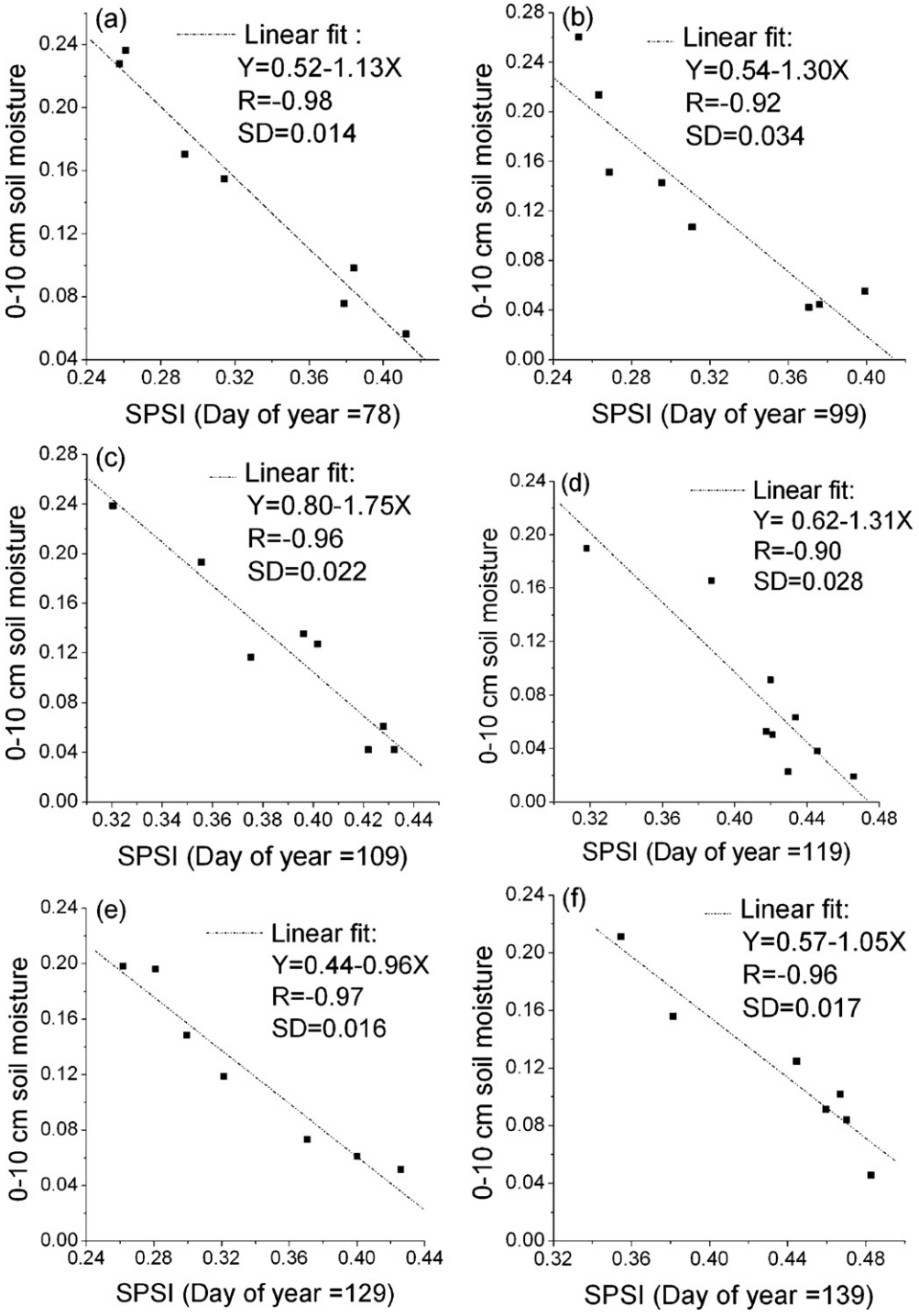

Fig. 4. (a)–(h) The relationship between SPSI and ground 0–10 cm soil moisture measurements at Ningxia province of China, from March 18, 2004 (Day of year 78) to June 18, 2004 (Day of year 170) (SD and *R* are the standard deviation and correlation coefficient between SPSI and ground measurements).

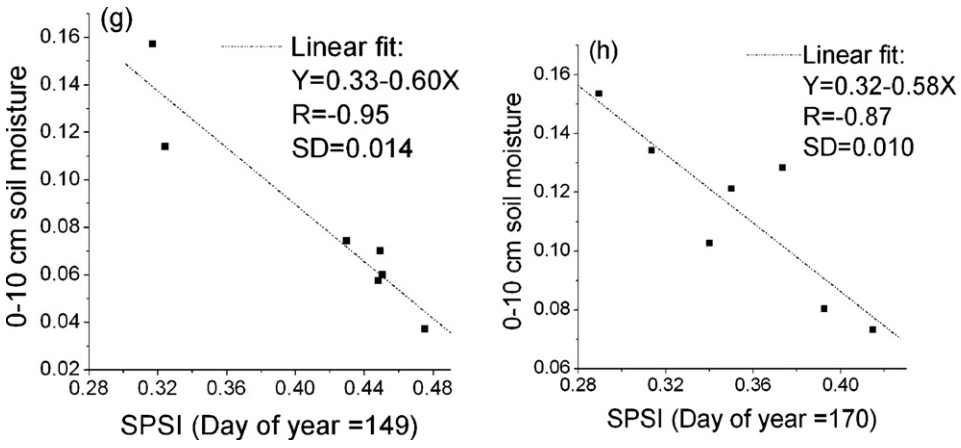

Fig. 4. (*Continued*).

et al., 2008). The EnKF applies a so-called Markov Chain Monte Carlo (MCMC) method to solve the time evolution of the probability density of model states (Evensen, 2003). With the Monte Carlo framework, the model states/parameters are perturbed to account for model errors (Hamill and Whitaker, 2005; McLaughlin et al., 2006)

$$x_{t+1}^{j} = M(x_t + \varepsilon_t^j), \quad \varepsilon^j \sim N(0, R_x), \quad j = 1, \ldots, N \tag{14}$$

where x_t represents the model states/parameters at time t; ε_t^j is a random noise with a Gaussian probability distribution added to x_t; x_{t+1}^j is the jth realization of model states/parameters at time t + 1. M is an ecological process model and represents the BEPS model in our case.

BEPS has been evaluated in several comprehensive studies (Liu et al., 2003; Feng et al., 2007) at forest areas located in Canada and China at 1 km resolution. Thus we consider the conceptual aspects (including equations and principles) of BEPS are valid and the spatial resolution is feasible. At the local scale, model forcing data are measured with sufficient accuracy compared to the ecosystem parameter uncertainties. The model uncertainties derived from forcing data are not considered in this study. Therefore, we assume the model error for estimating soil moisture arises from model parameter errors including β and g_{max} which are closely related to the soil water balance.

As shown in Fig. 2, at the beginning of data assimilation, two key model parameters, β and g_{max}, are perturbed in BEPS to account for the model error. After the parameter optimization using EnKF, mean values and error covariances of updated parameter ensembles are calculated and are further used to perturb parameter ensembles of the next sub-period. In this way, we can account for the dynamics of model errors during the whole study period.

4. Model performance with the data assimilation scheme

The data assimilation strategy was used in the study area during the growing season with an ensemble of 200 realizations. Model performance was evaluated using the Nash–Sutcliffe model efficiency coefficient (Nash and Sutcliffe, 1970). It is defined as:

$$E = 1 - \frac{\sum_{t=1}^{T}(Q_0^t - Q_m^t)^2}{\sum_{t=1}^{T}(Q_0^t - \bar{Q}_0)^2} \tag{15}$$

where Q_0 is observation; Q_m is model prediction; $\bar{Q}_0$ represents the mean value of observation at time t; and T is the number of data assimilation sub-periods. In this study, T is equal to 8. The Nash–Sutcliffe model efficiency coefficient (E) ranges from $-\infty$ to 1. The closer the model efficiency is to 1, the more accurate the model is.

4.1. Point-based model performance and the influence of initial parameters and their standard deviations

The generation of the initial 0–10 cm soil moisture ensemble is realized by disturbing model parameters including *LAI*, g_{max} and β. Therefore, initial values of these parameters are crucial in successfully representing the real initial conditions of the model states (Mo et al., 2008). The initial values of g_{max} and β were carefully determined from the empirical ranges of crops in the study area. Since field measurements of these parameters are not available for validation, there are still considerable uncertainties linked to the initial values.

Point-based time-series of remotely sensed, model-predicted and assimilated 0–10 cm soil moisture from DOY 78 to DOY 170 at a crop site (106°16′E, 36°00′N) are shown in Fig. 5. As shown in Fig. 5(a), before data assimilation, the model-predicted 0–10 cm soil moisture deviates gradually from the observation. Precipitation has a large influence on the model estimation. Generally, in sub-periods with precipitation, BEPS overestimates the 0–10 cm soil moisture as compared to observations. While in sub-periods with no or little precipitation, BEPS underestimates the soil moisture. As demonstrated in Fig. 5(a), BEPS' estimation of 0–10 cm soil moisture after parameter optimization is improved in comparison with observations. The Nash–Sutcliffe model efficiency coefficient (E) for 0–10 cm soil moisture estimation after parameter optimization increases from 0.554 to 0.687.

The EnKF method has been tested in a weather forecast model to be robust even with poor estimates of initial model states (Zhang, 2004). Weerts and El Serafy (2006) also suggested that the EnKF method is less sensitive to misspecification of model parameters and input uncertainties than other nonlinear filters. To further investigate the influence of the initial values of model parameters on the soil moisture estimation using TSDA, case (b) to case (f) (Fig. 5(b)–(f)) are simulated. In these cases, other input parameters stay unchanged except for the initial g_{max} and β values and their standard deviations that vary in a way shown in Table 2. Initialization of these parameters and their standard deviations in BEPS has a slight influence on the model performance in the first several days. As seen in Fig. 5(b)–(f), during sub-period 1 (DOY 78–99), the difference between model prediction and observation varies considerably. However, over the whole modeling period (growing season), the total model performance is notably improved after parameter optimization, and

the final model results are little affected by the parameter initialization within reasonable ranges. From case (a) to (f), the average Nash–Sutcliffe model efficiency coefficient for the model prediction of 0–10 cm soil moisture (E^b) during the whole running period is 0.538, and after data assimilation, it increases to 0.696.

4.2. Improving assimilation results

From Fig. 5(a)–(f), we can see that the TSDA scheme performs well during most data assimilation cycles except for sub-period 6 (DOY 139–149) when the parameters stay almost unchanged after the parameter update, leading to little change in the surface

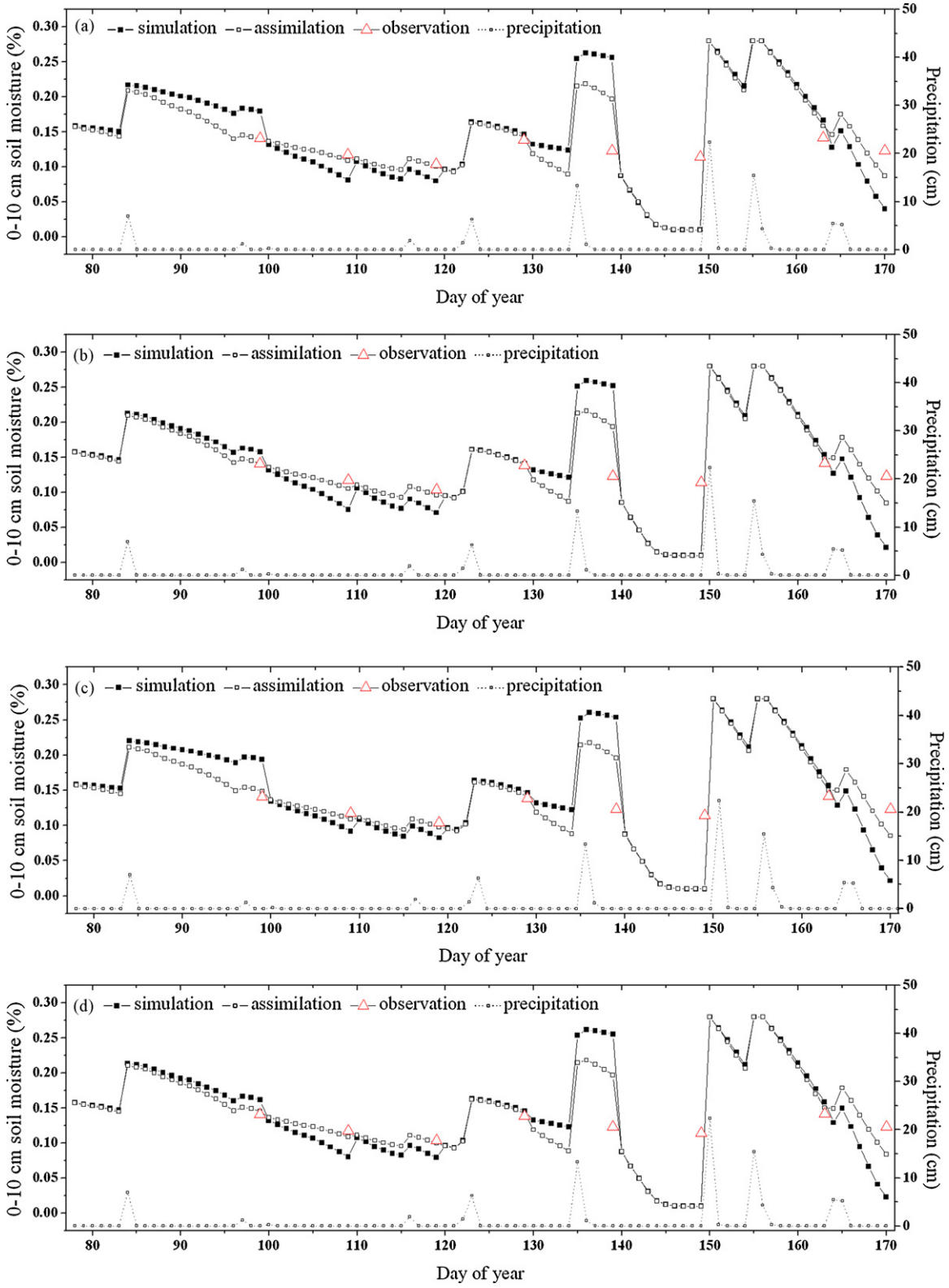

Fig. 5. (a)–(g) Comparison between model simulated and assimilated 0–10 cm soil moisture and observation.

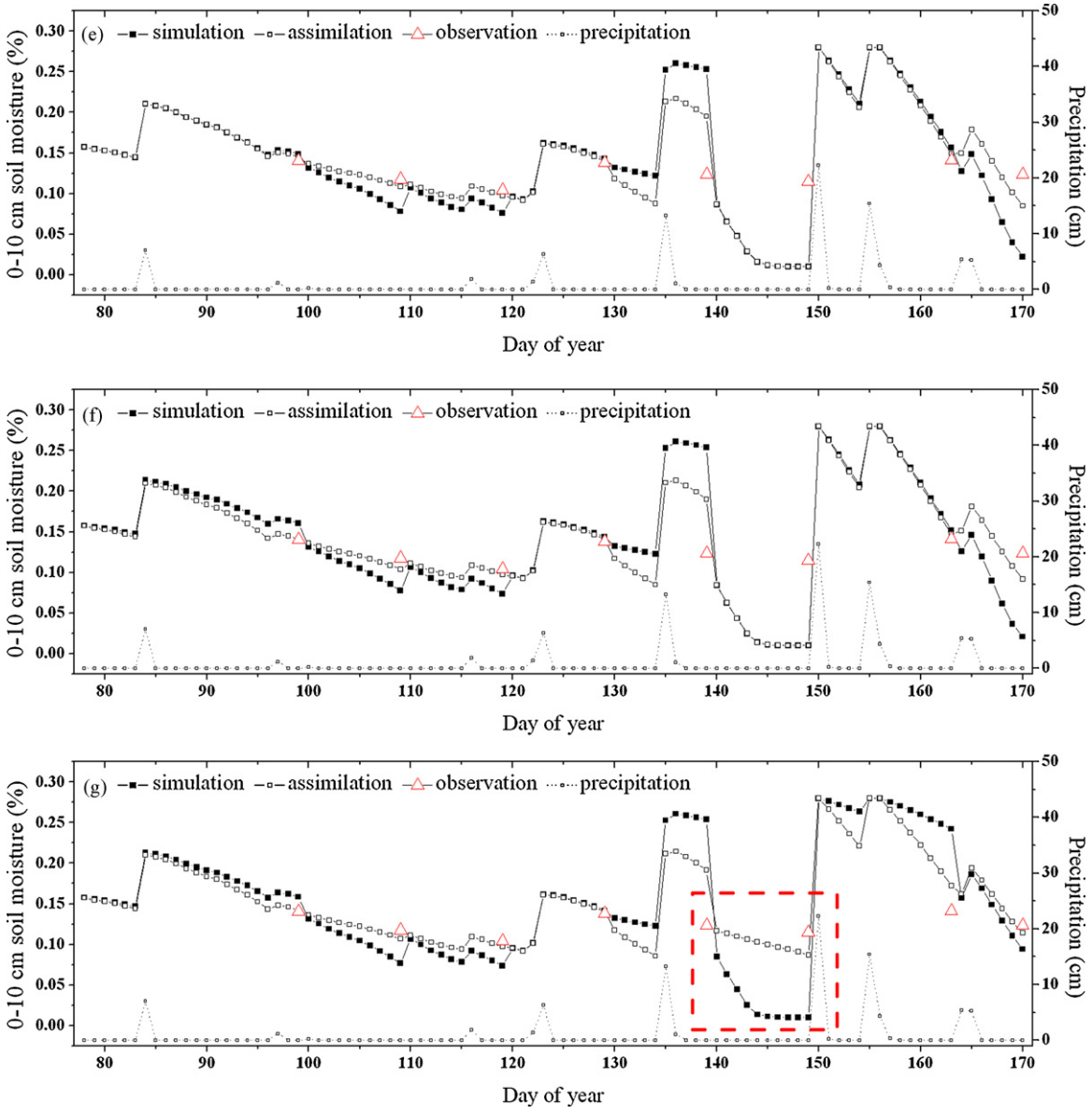

Fig. 5. (*Continued*).

0–10 cm soil moisture after data assimilation. There are two reasons for this phenomenon: (1) there is no precipitation during DOY 139–149, and the LAI and g_{max} are higher than earlier days. After several days in the model run, the 0–10 cm soil moisture was close to the wilting point, and in the model, the soil moisture at the top layer changes very little when the wilting point is reached. (2) When the 0–10 cm soil moisture reaches the wilting point, each element in the 0–10 cm soil moisture ensemble will become the same as the wilting point which leads to a zero deviation in the ensemble and makes the Kalman gain reduce quickly. As a result of this dryness, the soil moisture after data assimilation is almost unchanged.

Table 2
The influence of initial values and standard deviations of g_{max} and β to the model performance.

	Initial value	Standard deviation	E^b	E^a
Case (a)	g_{max} = 5 (mm s^{-1}) β = 0.94	2 0.003	0.554	0.687
Case (b)	g_{max} = 5 (mm s^{-1}) β = 0.91	2 0.003	0.538	0.696
Case (c)	g_{max} = 2 (mm s^{-1}) β = 0.91	2 0.003	0.521	0.704
Case (d)	g_{max} = 5 (mm s^{-1}) β = 0.91	2 0.003	0.538	0.687
Case (e)	g_{max} = 5 (mm s^{-1}) β = 0.91	5 0.003	0.543	0.686
Case (f)	g_{max} = 5 (mm s^{-1}) β = 0.91	2 0.005	0.532	0.714
Case (g)	g_{max} = 5 (mm s^{-1}) β = 0.91	2 0.003	0.530	0.895

It has been recognized that the linear updating mechanism and normality approximations of the EnKF may lead to biases or imbalances of output state variables within a model structure that is strongly nonlinear (Zhou et al., 2006; Weerts and El Serafy, 2006; Pan and Wood, 2006; Moradkhani, 2004, 2008). Pan and Wood (2006) developed a Constrained Ensemble Kalman Filter (CEnKF), in which the EnKF is used twice to optimally redistribute any imbalance from the first step. However, when a model indicates soil water stress, the model ensemble may lose a large part of its statistical properties, leading to ineffectiveness of the EnKF.

In this study, we developed a simple method to fine-tune g_{max} to account for extreme water conditions in the model. That is, each time before performing the EnKF, the model will first be checked if the deviation of 0–10 cm soil moisture is reduced to zero and if the

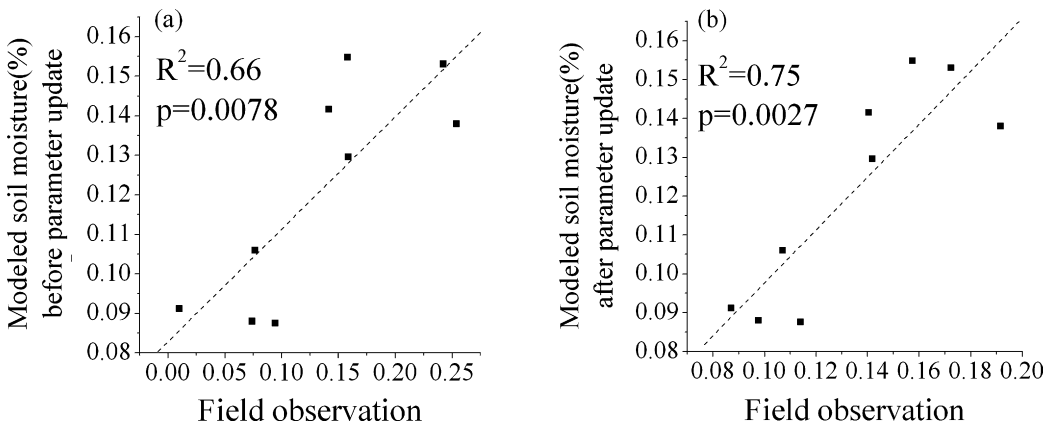

Fig. 6. (a) and (b) Modeled surface soil moisture compared with field observations.

difference between observed and simulated 0–10 cm soil moisture is positive. If it is, g_{max} is directly decreased to 50% of its original value to amend the unreasonable excessive water loss in the model, and the EnKF is quitted in the present sub-period. Fig. 5(g) shows the result after this modification, using updated g_{max} together with other parameters, at DOY 149, the model simulated result increases considerably in accord with the observation. Correspondingly the Nash–Sutcliffe model efficiency coefficient increases from 0.530 before the parameter update to 0.895 after the parameter update.

4.3. Field validation of the optimized model

Scatter plots of model-predicted vs. observed values is the most commonly used approach to evaluate model predictions (Mesple et al., 1996; Piñeiro et al., 2008). Model-simulated 0–10 cm soil moisture is compared with field measurements using the scatter plot method. There is one field measurement (106.16°E, 36.00°N) of 0–10 cm soil moisture within each data assimilation cycle. For the whole study period (DOY 78–170), there are 9 field measurements in total. The correlation between the model and field measurements increases from 0.66 (before the parameter update) to 0.75 (after the parameter update) as shown in Fig. 6, which demonstrates that the data assimilation scheme developed in this study is effective in improving the model performance using remote sensing observations.

4.4. Spatial evaluation of model performance

The spatial distribution of the Nash–Sutcliffe model efficiency coefficient for modeled 0–10 cm soil moisture displays pronounced east-west and north-south gradients as well as detailed variation

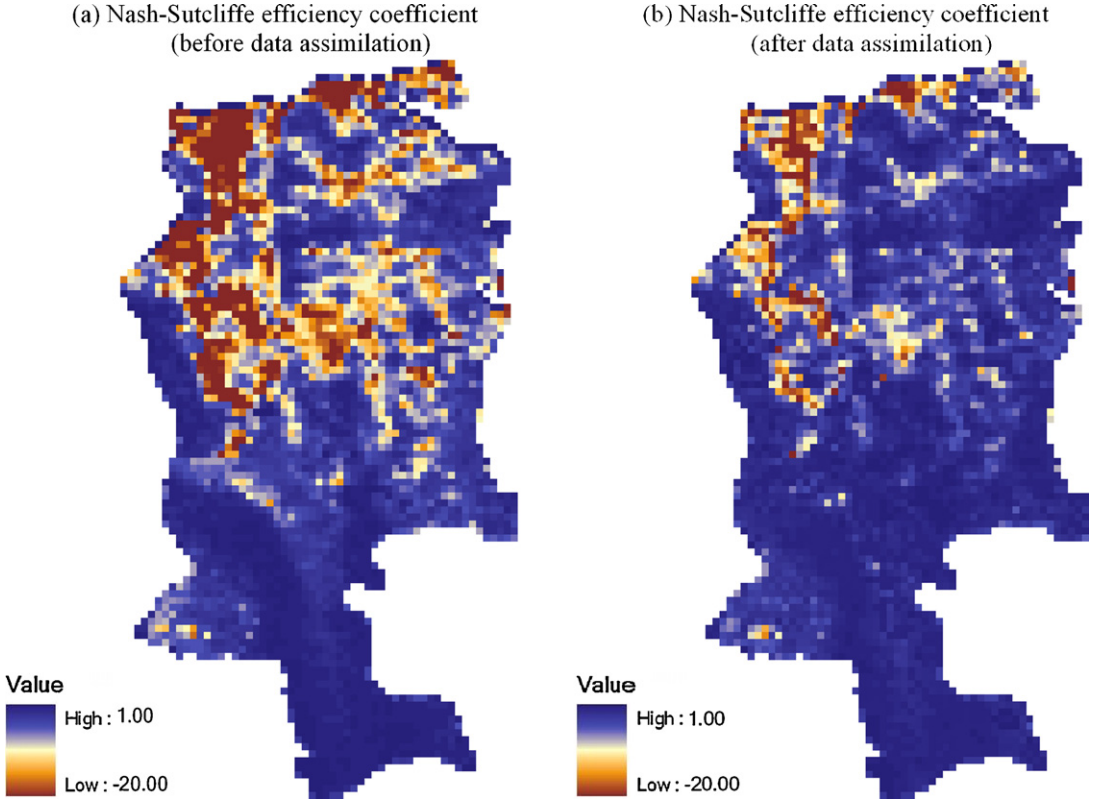

Fig. 7. (a) and (b) Agreement index before and after parameter optimization.

with land cover type and vegetation density. As shown in Fig. 7(a), 0–10 cm soil moisture simulated by the model before the parameter optimization is relatively close to the observation in the southern part of the study area where the dominant vegetation type is forest and spring wheat. While in the northern part of the study area, the model performance is much poorer, especially near the west boundary of the study area with the Nash–Sutcliffe model efficiency coefficient lower than 0. Land cover types in the northern part of the study area are mainly sparse grass and crop. In comparison with Fig. 7(a), we can see that after data assimilation and parameter optimization, as shown in Fig. 7(b), the Nash–Sutcliffe model efficiency coefficient has been improved significantly, especially in the northern and middle parts of the study area. These results demonstrate that the two-stage data assimilation scheme is effective in improving the day-to-day surface soil moisture estimation.

However, it should be noted that in the northeast part of the study area, the model performance is not much improved after parameter optimization. Through further investigation, we found that parameters including g_{max} and β almost stay unchanged during the data assimilation, leading to little change in the 0–10 cm soil moisture after parameter optimization. The uncertainty of soil hydraulic conductivity in BEPS is the main reason for the critical model performance in this area. Soil hydraulic conductivity is a very important parameter in the Penman–Monteith equation for estimating evaporation from soil. In areas where the land surface is covered by dense vegetation, evaporation from soil is very low. However, in areas where the vegetation cover fraction is very low, evaporation from the soil surface is the main process influencing soil water balance. In this study, our focus is on optimizing two key parameters of BEPS (including g_{max} and β) which influence canopy transpiration while the spatial and temporal uncertainties of soil conductance are ignored. As shown in Fig. 8, after data assimilation, the model performance is still very poor in the northwest part of the study area where the average LAI during the whole study period is very low (where the land cover types are sparse grass and crop as shown in Fig. 9).

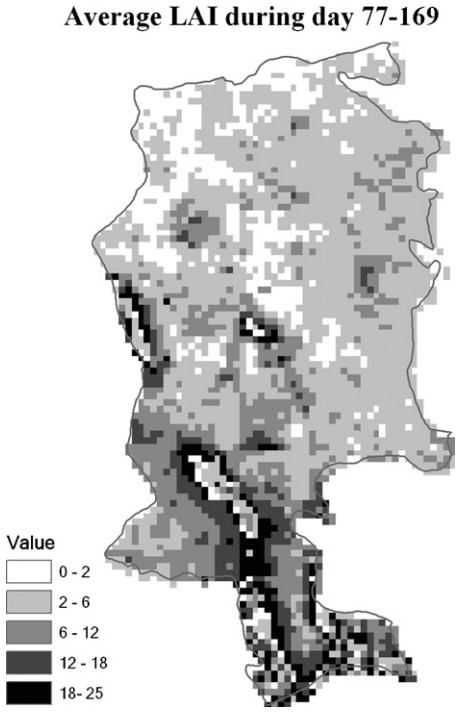

Fig. 8. Average LAI during the whole study period.

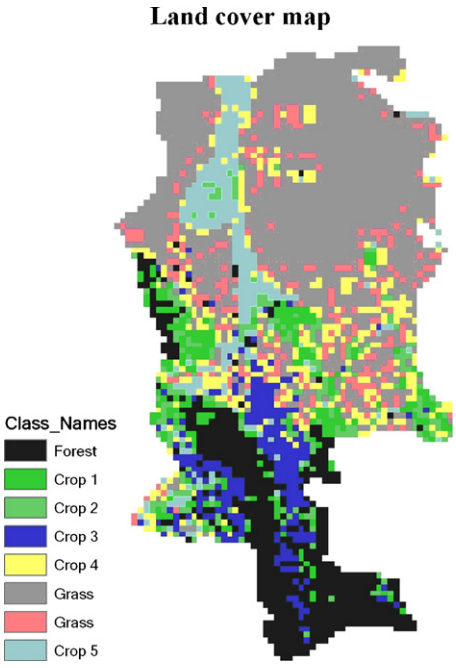

Fig. 9. Land cover map of study area.

5. Temporal and spatial variation of model parameters

For further exploring the variations of model parameters after parameter optimization, a sub-area in the study area (Fig. 3) is extracted and its temporal and spatial variations are examined. Compared to other locations of the study area, the Nash-Sutcliffe model efficiency coefficient in this sub-area improved most significantly after parameter optimization. Therefore it would be useful to further examine the temporal and spatial changes of optimized parameters.

5.1. Temporal variation of parameters

During each data assimilation cycle, the average values of the maximum stomatal conductance (g_{max}) and root depth coefficient (β) of the sub-area are computed and the temporal variations of these two parameters during the 8 sub-periods are displayed in Fig. 10. Results show that g_{max} and β vary significantly with time. Generally, g_{max} and β are found to be negatively correlated, and both have a decreasing trend with time.

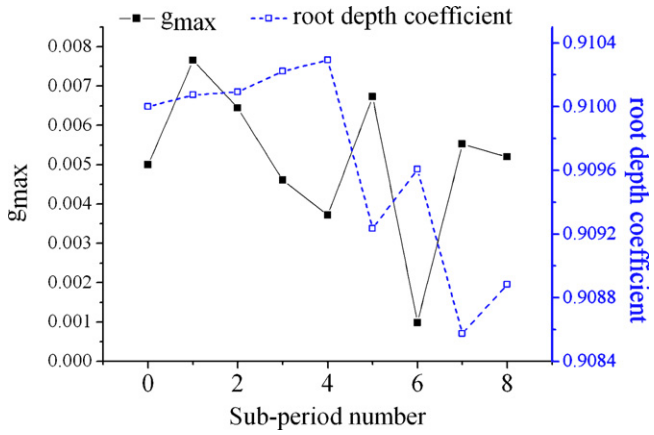

Fig. 10. Temporal variation of parameters during the study period.

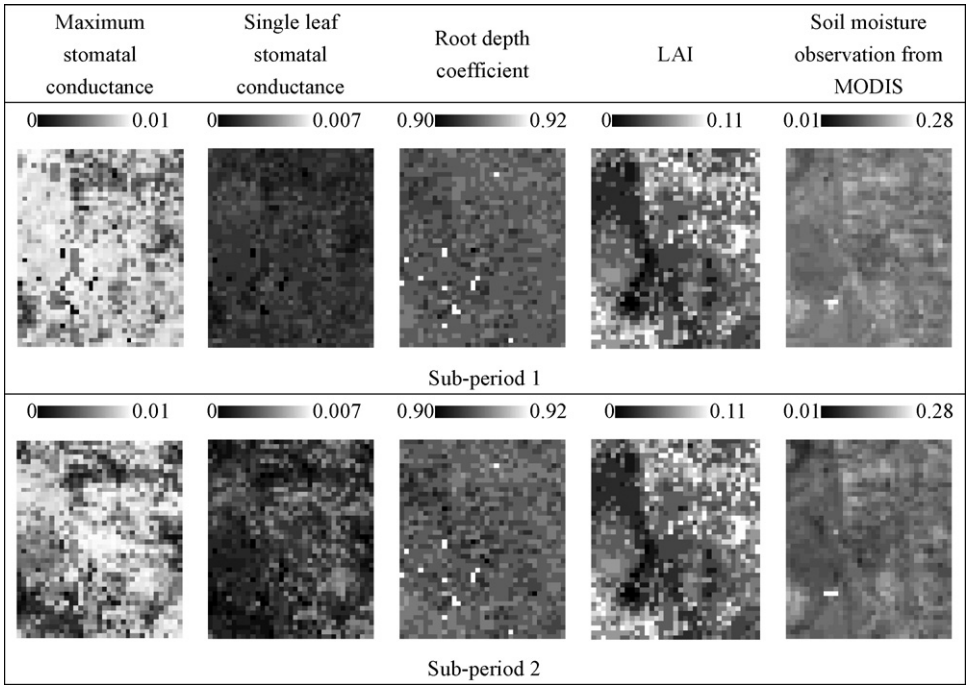

Fig. 11. Spatial distribution of model parameters at the sub-area (sub-periods 1 and 2).

Stomatal conductance is an important factor that affects transpiration (Maruyama and Kuwagata, 2008; Fischer et al., 2008). Generally, stomata close in response to drought and open when the atmospheric vapor pressure deficit is low (Socias et al., 1997; Endres, 2007; Mo et al., 2008). Endres (2007) reported that younger leaves displayed greater stomatal conductance. In this study, the decreasing trend of g_{max} with time gave support to Endres's finding. Furthermore, comparing Fig. 10 to Fig. 5, we found that during sub-periods when modeled soil moisture is low (such as sub-period 6), g_{max} has a sharp decrease. While during sub-periods 5 and 7 with plenty precipitation, g_{max} increases quickly. Although the Jarvis method includes scalar functions that take in to account the instantaneous effects of soil water content and atmospheric vapor deficit on leaf stomatal conductance by scaling down the actual stomatal conductance from the given maximum value accordingly, the detrimental effects of long and persistent droughts on plant leaves (including leaf pigments and nutrient status) could not be well captured with the fixed g_{max} values. By allowing g_{max} to vary temporally, these detrimental effects are included. The variation of g_{max} with time demonstrated that the data assimilation scheme

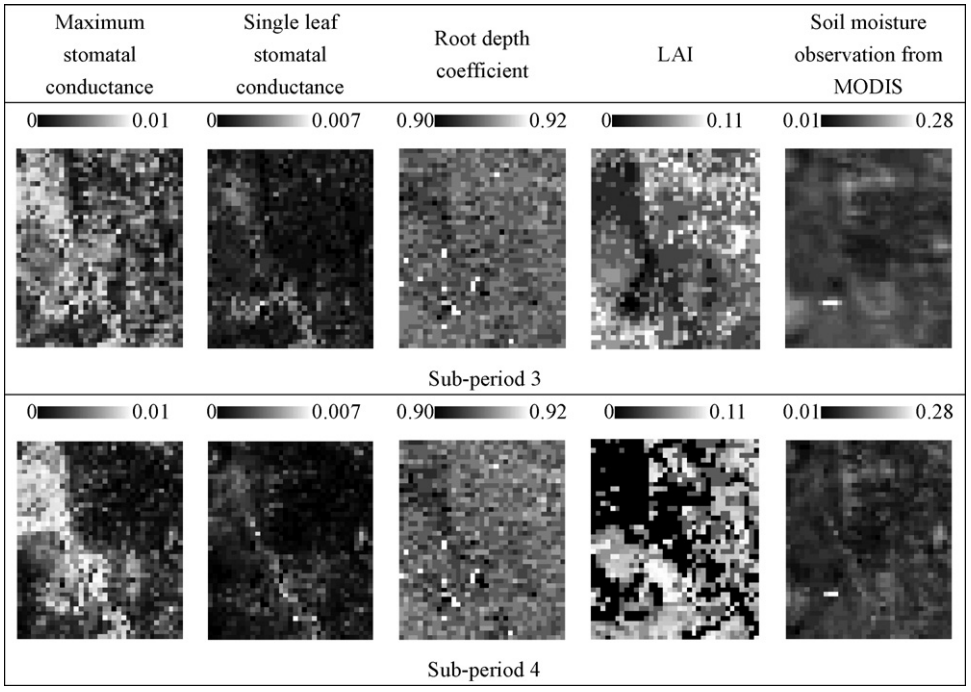

Fig. 12. Spatial distribution of model parameters at the sub-area (sub-periods 3 and 4).

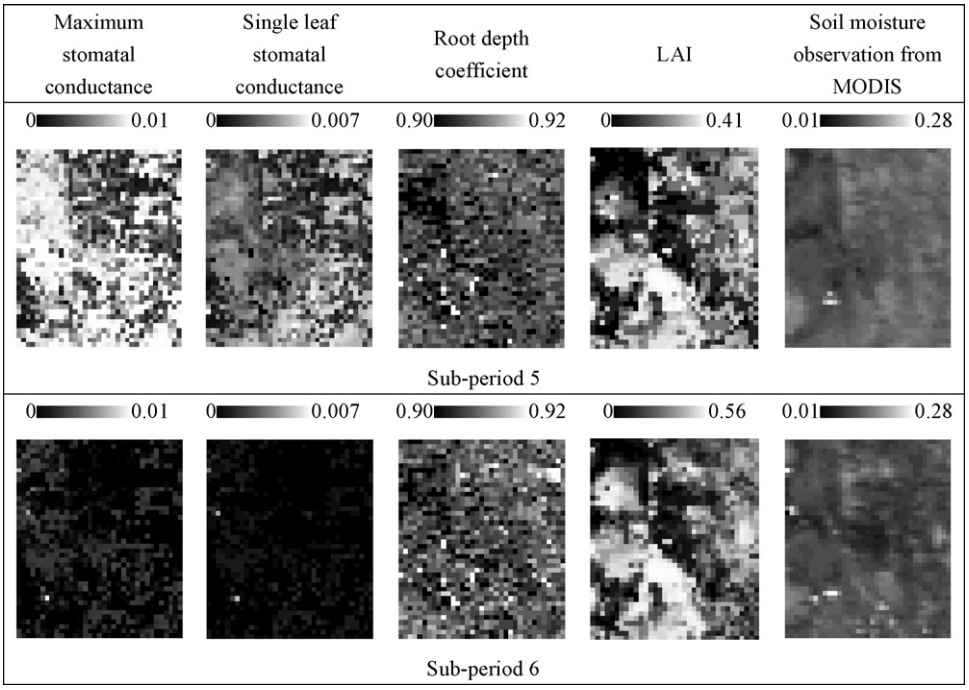

Fig. 13. Spatial distribution of model parameters at the sub-area (sub-periods 5 and 6).

developed in the study has the ability to control the response of stomatal movement to persistent environment changes that affect plant health status.

In BEPS, the root depth coefficient (β) is used to compute the root vertical distribution within each soil layer. Accurate estimation of β is helpful to understand plant rooting patterns and therefore is a very important parameter in ecosystem modeling (Jackson et al., 1996). Although in reality, the rooting pattern for a specific plant varies with plant growth and also with environmental change, in previous ecological modeling, β is often set as a constant. For crop and grassland area, Jackson et al. (1996) reported that the typical value for β is around 0.91–0.96. Considering that, the model is initialized in early stage of vegetation growth (from DOY = 78 of 2004) when a large part of the roots is distributed in top 30 cm of the soil, the initial β is set as 0.91 for the sub-area. As shown in Fig. 10, during the latter four sub-periods, β fluctuates quickly and have a decreasing trend with time. The quick variation of β shows that modeled soil moisture has a great influence on β. When the modeled soil moisture is very low (such as sub-period 6), β is increased to have more proportion of transpiration originating from

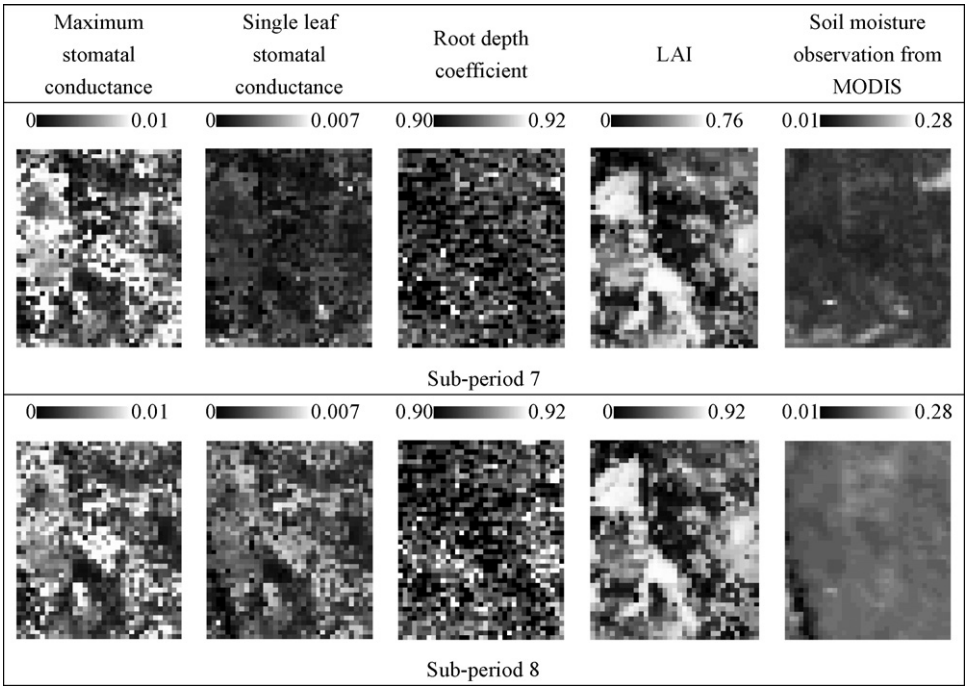

Fig. 14. Spatial distribution of model parameters at the sub-area (sub-periods 7 and 8).

the deeper soil. While when the modeled soil moisture is high (during sub-periods 5 and 7), the soil moisture in the upper soil layer is enough to support canopy transpiration, and β decreases correspondingly. Therefore, the TSDA scheme appears to be able to capture the temporal variation pattern of plant root water extraction in the model.

The temporal variation patterns of the above two parameters can be further explained by the regulation mechanism in the EnKF updating equation. As shown in Eq. (11), there are two driving factors in the EnKF updating process which collectively influence the extents to which parameters can be modified. The first factor is the difference between observed and modeled 0–10 cm soil moisture, which is termed innovation in Eq. (11). The second factor is the Kalman gain for each parameter. Considering that at each parameter updating process, innovation is the same for g_{max} and β, the corrections made to the model parameters are determined by their corresponding Kalman gains. In BEPS, g_{max} is negatively correlated to 0–10 cm soil moisture while β is positively correlated to 0–10 cm soil moisture. Correspondingly, the Kalman gain in Eq. (12) for g_{max} is negative and for β is positive. This is the reason that these two parameters are updated in the opposite directions.

5.2. Spatial patterns of parameters

As shown in Figs. 11–14, during each sub-period, there are meaningful spatial distributions of g_{max}, single leaf g (single leaf stomatal conductance) and β after parameter updating in the spatial mode, which can be summarized as following:

1. In BEPS, *LAI* is an important factor that relates single leaf conductance and canopy transpiration using a sunlit and shaded leaf separation method (Chen et al., 1999; Liu et al., 2003). In this study, the spatial distribution of stomatal conductance is estimated through assimilating remotely sensed soil moisture into BEPS-simulated soil moisture. From Figs. 11–14, we can see that at the time scale of several days, using the TSDA scheme, vegetation dynamics (in terms of the *LAI* series in this study) show an influence on the temporal variation of g_{max} and its spatial pattern via soil moisture that controls transpiration, especially when *LAI* is higher than 0.2. During periods when the observed soil moisture and other meteorological conditions do not change much, *LAI* is the primary factor influencing the variation of g_{max}. The relationship between *LAI* and stomatal conductance helps to understand the physical mechanisms controlling the spatial and temporal variations of these two parameters. Generally, considering that an increase in *LAI* can sometimes force stomatal opening to decrease or even close to prevent excessive water loss in plants, it is reasonable to find that g_{max} decreases with increasing LAI in some cases, especially in sub-periods 3, 7 and 8.
2. Comparing between the time series of *LAI* and 0–10 cm soil moisture maps, we conclude that the spatial distribution of observed soil moisture and its evolution with time is affected by the regional vegetation to some extent. Especially in sub-periods 1, 5 and 6, a positive feedback could exist between *LAI* and soil moisture, which reinforces similar findings of the studies of Rodriguez-Iturbe et al. (1999), D'Odorico et al. (2007) and Arora (2002).
3. During the growing season, leaf-level g is not only affected by meteorological conditions but also by soil moisture (Barradas et al., 1994; Ewers et al., 2001). In this study, the calculation of leaf-level g is based on the modified Javis' model which considers the influence of daily soil moisture variation on g. As displayed in the times series of 0–10 cm soil moisture maps and leaf-level g maps (Figs. 11–14), the spatial distribution of g is positively correlated with the spatial variation of 0–10 cm soil moisture. This positive relationship demonstrates that the modified Javis' model has the ability to capture the influence of surface dryness or wetness on the leaf-level g. Through parameter optimization and Javis' model modification, the updated g becomes reasonably sensitive to the environmental influence. Thus it can be concluded that the TSDA scheme is effective in improving leaf-level stomatal conductance estimation both temporally and spatially.
4. Distinct from g_{max}, there is no spatially explicit pattern in the variation of β, while the average β of the whole sub-area exhibits a decreasing trend with increasing spatial heterogeneity with time. The lack of a spatial pattern indicates that β is not as sensitive as g_{max} to the surface soil moisture, making the average β of the whole sub-area change little with time. The decrease of β indicates an increased proportion of roots near the soil surface which contributes to the total transpiration. One reason for this decrease is that with the growth of vegetation, the heterogeneity of the land surface is increasing. Another reason is the distribution of precipitation. Especially during sub-periods 5, 7, and 8, there are relatively large amounts of precipitation in this area, which lead to sharp increases in the surface soil moisture, as well as increases in the proportion of transpiration from the top soil layer.

6. Summary and conclusions

Our study demonstrates the feasibility of assimilating remotely sensed surface soil moisture data into an ecosystem model (BEPS) in an arid and semi-arid area of northwest China to improve the performance of soil moisture prediction in that area. A two-stage data assimilation scheme is developed to fine-tune two key model parameters using the Ensemble Kalman Filter and to reinitialize the model to get improved predictions of 0–10 cm soil moisture. The model performance using TSDA is first tested and validated using field 0–10 cm measurements at a site. The influence of initial values of model parameters and their standard deviations on model performance is also investigated. Using remotely sensed top 10 cm soil moisture, the spatial and temporal distribution of the same model parameters is also optimized. Through this study, the following conclusions are drawn:

(1) The TSDA scheme developed in this study is robust and effective for spatial and temporal optimization of some key model parameters and considerably improves the estimation of 0–10 cm soil moisture except for extremely dry conditions, i.e. soil moisture near the wilting point estimated in the model.
(2) Initialization of parameter values and their standard deviations in BEPS has a slight influence on the model performance in the first several days (sub-period). However, over the whole modeling period (growing season), the total model performance is notably improved after parameter optimization. The final model results are little affected by the parameter initialization within reasonable ranges.
(3) Spatially, the TSDA method results in significant improvement in model performance in most areas except for areas where *LAI* is very low. In these very sparsely vegetated areas, it is evaporation from the soil surface rather than the transpiration that affects soil moisture. Considering the dynamics of soil hydraulic conductivity that affects evaporation in the optimization scheme would potentially further improve the model performance in very sparsely vegetated areas.
(4) The TSDA scheme can help not only reveal the temporal and spatial variations of model parameters but also understand the corresponding ecological mechanisms controlling these variations. Temporally, g_{max} and β vary significantly during each parameter updating stage, and the TSDA scheme is effective in

capturing their temporal variations and the mutual compensating effects of these two parameters. Spatially, TSDA is helpful for revealing the spatial variations of the BEPS model parameters. Input *LAI* series and 0–10 cm soil moisture observations influence the spatial distributions of optimized model parameters and are useful for the optimization and application of the ecosystem model to large areas.

This study is only focused on optimizing two key parameters of BEPS (including g_{max} and β) which influence canopy transpiration while the spatial and temporal uncertainties of other model parameters are ignored. In the future work, a parameter sensitivity analysis is yet to be done to analyze the model more thoroughly. In addition, further research is required to improve the accuracy of remotely sensed surface soil moisture to provide a more reliable spatial observation.

Acknowledgements

We would like to acknowledge several scientists who developed the BEPS model and the data assimilation scheme, particularly Dr. Xingguo Mo who developed the code for implementing EnKF and Dr. Ajit Govind who helped implement the final algorithm during the 1-year training of the senior author at the University of Toronto. This research is supported by the National Natural Science Foundation of China (No. 40771148), the State Scholarship Fund of China (2007U01086) and the Special Fund for Public Welfare Industry of China (Meteorology) (GYHY200806022).

References

Arora, V.K., 2002. Modeling vegetation as a dynamic component in soil-vegetation-atmosphere transfer schemes and hydrological models. Rev. Geophys. 40 (2), 1006.

Bach, H., Mauser, W., 2003. Methods and examples for remote sensing data assimilation in land surface process modeling. IEEE Trans. Geosci. Remote Sens. 41 (7), 1629–1637.

Barradas, V.L., Jones, H.G., Clark, J.A., 1994. Stomatal responses to changing irradiance in Phaseolus vulgaris L. J. Exp. Bot. 45, 931–936.

Braswell, B.H., Sacks, W.J., Linder, E., Schimel, D.S., 2005. Estimating diurnal to annual ecosystem parameters by synthesis of a carbon flux model with eddy covariance net ecosystem exchange observations. Global Change Biol. 11, 335–355.

Burgers, G., Van Leeuwen, P.J., Evensen, G., 1998. Analysis scheme in the ensemble Kalman filter. Monthly Weather Rev. 126, 1719–1724.

Chen, B., Chen, J.M., Ju, W., 2007. Remote sensing-based ecosystem–atmosphere simulation scheme (EASS)—model formulation and test with multiple-year data. Ecol. Model., 277–300.

Chen, J.M., Liu, J., Cihlar, J., Coulden, M.L., 1999. Daily canopy photosynthesis model through temporal and spatial scaling for remote sensing applications. Ecol. Model. 124, 99–119.

Chen, J.M., Chen, X., Ju, W., Geng, X., 2005. Distributed hydrological model for mapping evapotranspiration using remote sensing inputs. J. Hydrol. 305, 15–39.

Deng, F., Chen, J.M., Plummer, S., Chen, M., Pisek, J., 2006. Algorithm for global leaf area index retrieval using satellite imagery. IEEE Trans. Geosci. Remote Sens. 44, 2219–2229.

Dorigo, W.A., Zurita-Milla, R.D.E., Wit, A.J.W., Brazile, J., Singh, R., Schaepman, M.E., 2007. A review on reflective remote sensing and data assimilation techniques for enhanced agroecosystem modeling. Int. J. Appl. Earth Obs. Geoinf. 9, 165–193.

D'Odorico, P., Caylor, K., Okin, G.S., Scanlon, T.M., 2007. On soil moisture–vegetation feedbacks and their possible effects on the dynamics of dryland ecosystems. J. Geophys. Res. 112, G04010, doi:10.1029/2006JG000379.

Eitzinger, J., Trnka, M., Hösch, J., Žalud, Z., Dubrovský, M., 2004. Comparison of CERES WOFOST and SWAP models in simulating soil water content during growing season under different soil conditions. Ecol. Model. 171, 223–246.

Endres, L., 2007. Daily and seasonal variation of water relationship in sugar apple (Annona squamosa L.) under different irrigation regimes at semi-arid Brazil. SCI Hortic-Amsterdam. 113, 149–154.

Entekhabi, D., Nakamura, H., Njoku, E.G., 1994. Solving the inverse problem for soil moisture and temperature profiles by sequential assimilation of multifrequency remotely sensed observations. IEEE Trans. Geosci. Remote Sens. 32, 438–448.

Evensen, G., 1994. Sequential data assimilation with a non-linear quasi-geostrophic model using Monte Carlo methods to forecast error statistics. J. Geophys. Res. 99 (C5), 10143–10162.

Evensen, G., 2003. The ensemble Kalman filter: theoretical formulation and practical implementation. Ocean Dyn. 53, 343–367.

Ewers, B.E., Oren, R., Johnsen, K.H., Landsberg, J.J., 2001. Estimating maximum mean canopy stomatal conductance for use in models. Can. J. For. Res. 31, 198–207.

Feng, X., Liu, G., Chen, J.M., Chen, M., Liu, J., Ju, W.M., Sun, R., Zhou, W., 2007. Net primary productivity of China's terrestrial ecosystems from a process model driven by remote sensing. J. Environ. Manage. 85, 563–573.

Fischer, B., Goldberg, V., Bernhofer, C., 2008. Effect of a coupled soil water–plant gas exchange on forest energy fluxes: simulations with the coupled vegetation–boundary layer model HIRVAC. Ecol. Model. 241, 75–82.

Gale, M.R., Grigal, D.F., 1987. Vertical root distributions of northern tree species in relation to successional status. Can. J. Forest Res. 17, 829–834.

Ghulam, A., Qin, Q., Teyip, T., Li, Z.L., 2007a. Modified perpendicular drought index (MPDI): a real-time drought monitoring method. ISPRS J. Photogramm. 62, 150–164.

Ghulam, A., Li, Z.L., Qin, Q., Tong, Q., Wang, J., Alimujiang, K., Lin, Z., 2007b. A method for canopy water content estimation for highly vegetated surfaces–shortwave infrared perpendicular water stress index. Sci. China, Ser. D 50 (9), 1359–1368.

Ghulam, A., Qin, Q., Zhan, Z., 2007c. Designing of the perpendicular drought index. Environ. Geol. 52 (6), 1045–1052.

Ghulam, A., Li, Z.L., Qin, Q., Yimit, H., Wang, Y., 2008. Estimating crop water stress with ETM+ NIR and SWIR data. Agric. Forest Meteorol. 148, 1679–1695.

Gillies, R.P., 1997. A verification of the "triangle" method for obtaining surface soil water content and energy fluxes from remote measurements of the Normalized Difference Vegetation Index (NDVI) and surface radiant temperature. Int. J. Remote Sens. 18 (15), 3145–3166.

Hamill, T.M., Whitaker, J.S., 2005. Accounting for the error due to unresolved scales in ensemble data assimilation: a comparison of different approaches. Monthly Weather Rev. 133, 3132–3147.

Hanson, J.D., Ahuja, L.R., Shaffer, M.D., Rojas, K.W., DeCoursey, D.G., Farahani, H., Johnson, K., 1998. RZWQM: simulating the effects of management on water quality and crop production. Agric. Syst. 57, 161–195.

Heathman, G.C., Starks, P.J., Ahuja, L.R., Jackson, T.J., 2003. Assimilation of surface soil moisture to estimate profile soil water content. J. Hydrol. 279, 1–17.

Hoeben, R., Troch, P.A., 2000. Assimilation of active microwave observation data for soil moisture profile estimation. Water Resour. Res. 36, 2805–2819.

Houser, P.R., Shuttleworth, W.J., Famiglietti, J.S., Gupta, H.V., Syed, K.H., Goodrich, D.C., 1998. Integration of soil moisture remote sensing and hydrologic modeling using data assimilation. Water Resour. Res. 34, 3405–3420.

Huang, C., Li, X., Lu, L., 2008. Retrieving soil temperature profile by assimilating MODIS LST products with ensemble Kalman filter. Remote Sens. Environ. 112, 1320–1336.

Jackson, R.B., Canadell, J., Ehleringer, J.R., Mooney, H.A., Sala, O.E., Schulze, E.D., 1996. A global analysis of root distributions for terrestrial biomes. Oecologia 108, 389–411.

Jarvis, P.G., Morison, J.I.L., 1981. Stomatal control of transpiration and photosynthesis. In: Jarvis, P.G., Mansfield III, T.A. (Eds.), Stomatal Physiology. Cambridge University Press, New York, pp. 247–279.

Ju, W., Chen, J.M., Black, T.A., et al., 2006. Modelling multi-year coupled carbon and water fluxes in a boreal aspen forest. Agric. For. Meteor. 140, 136–151.

Kalman, R.E., 1960. A new approach to linear filtering and prediction problem. Trans. ASME, Ser. D, J. Basic Eng. 82, 34–45.

Klute, A. (Ed.), 1986. Methods of Soil Analysis, Part 1, 2nd edition. American Society of Agronomy, Madison, WI.

Kogan, F.N., 1995. Application of vegetation index and brightness temperature for drought detection. Adv. Space Res. 15, 91–100.

Kostov, K.G., Jackson, T.J., 1993. Estimating profile soil moisture from surface layer measurements—a review. Ground Sens. 1941, 125–136.

Kuroda, H., Kishi, M.J., 2004. A data assimilation technique applied to estimate parameters for the NEMURO marine ecosystem model. Ecol. Model. 172, 69–85.

Li, J., Islam, S., 2002. Estimation of root zone soil moisture and surface fluxes partitioning using near surface soil moisture measurements. J. Hydrol. 259, 1–14.

Liu, J., Chen, J.M., Cihlar, J., Park, W.M., 1997. A processed based boreal ecosystem productivity simulator using remote sensing inputs. Remote Sens. Environ. 62, 158–175.

Liu, J., Chen, J.M., Cihlar, J., 2003. Mapping evapotranspiration based on remote sensing: an application to Canada's landmass. Water Resour. Res. 39, 1189.

Mandel, J., 2007. A brief tutorial on the Ensemble Kalman Filter, UCDHSC/CCM report No. 242.

Maruyama, A., Kuwagata, T., 2008. Diurnal and seasonal variation in bulk stomatal conductance of the rice canopy and its dependence on developmental stage. Agric. For. Meteorol. 148, 1161–1173.

McLaughlin, D., Zhou, Y.H., Entekhabi, D., Chatdarong, V., 2006. Computational issues for large scale land surface data assimilation problems. J. Hydrometeorol. 7 (3), 494–510.

Mcvicar, T.R., Jupp, D.L.B., 1998. The current and potential operational uses of remote sensing to aid decisions on drought exceptional circumstances in Australia: a review. Agr. Syst. 57 (3), 399–468.

Mesple, F., Troussellier, M., Casellas, C., Legendre, P., 1996. Evaluation of simple statistical criteria to qualify a simulation. Ecol. Model. 88, 9–18.

Mitchell, H., Houtekamer, P.L., 2002. Ensemble size, balance, and model-error representation in an Ensemble Kalman Filter. Monthly Weather Rev. 130, 2791–2808.

Mo, X., Chen, J.M., Ju, W., Andrew Black, T., 2008. Optimization of ecosystem model parameters through assimilating eddy covariance flux data with an Ensemble Kalman Filter. Ecol. Model. 217, 157–173.

Monteith, J.L., 1965. Evaporation and environment. Symposia Soc. Exp. Biol. 19, 205–234.

Moradkhani, H., 2004. Improved uncertainty assessment of hydrologic models using data assimilation and stochastic filtering. Ph.D. dissertation, University of California.

Moradkhani, H., 2008. Hydrologic remote sensing and land surface data assimilation. Sensors 8, 2986–3004.
Nash, J.E., Sutcliffe, J.V., 1970. River flow forecasting through conceptual models. 1. A discussion of principles. J. Hydrol. 10, 282–290.
Naud, C., Makowski, D., Jeuffroy, M., 2007. Application of an interacting particle filter to improve nitrogen nutrition index predictions for winter wheat. Ecol. Model. 207, 251–263.
Njoku, E.G., Li, L., 1999. Retrieval of land surface parameters using passive microwave measurements at 6-18 GHz. IEEE Trans. Geosci. Remote Sens. 37, 79–93.
Pan, M., Wood, E.F., 2006. Data assimilation for estimating the terrestrial water budget using a constrained Ensemble Kalman Filter. J. Hydrometeorol. 7, 534–547.
Piñeiro, G., Perelman, S., Guerschman, J.P., Paruelo, J.M., 2008. How to evaluate models: Observed vs. predicted or predicted vs. observed? Ecol. Model. 216, 316–322.
Pipunic, R.C., Walker, J.P., Western, A., 2008. Assimilation of remotely sensed data for improved latent and sensible heat flux prediction: a comparative synthetic study. Remote Sens. Environ. 112, 1295–1305.
Price, J.C., 1985. On the analysis of thermal infrared imagery: the limited utility of apparent thermal inertia. Remote Sens. Environ. 18, 59–73.
Quaife, T., Lewis, P., Kauwe, M.D., Williams, M., Law, B.E., Disney, M., Bowyer, P., 2008. Assimilation canopy reflectance data into an ecosystem model with an Ensemble Kalman Filter. Remote Sens. Environ. 112, 1347–1364.
Reichle, R.H., McLaughlin, D.B., Entekhabi, D., 2002a. Hydrologic data assimilation with the ensemble Kalman filter. Monthly Weather Rev. 130, 103–114.
Reichle, R.H., Walker, J.P., Koster, R.D., Houser, P.R., 2002b. Extended versus Ensemble Kalman Filtering for land data assimilation. J. Hydromet. 3, 728–740.
Reichle, R.H., Koster, R.D., Liu, P., Mahanama, S.P.P., Njoku, E.G., Owe, M., 2007. Comparison and assimilation of global soil moisture retrievals from the Advanced Microwave Scanning Radiometer for the Earth Observing System (AMSR-E) and the Scanning Multichannel Microwave Radiometer (SSMR). J. Geophys. Res. 112, D09108.
Raupach, M.R., Rayner, P.J., Barrett, D.J., Defries, R.S., Heimann, M., Jima, D.S.O., Quegan, S., Schmullius, C.C., 2005. Model-data synthesis in terrestrial carbon observation: methods, data requirements and data uncertainty specifications. Global Change Biol. 11, 378–397.
Rodriguez-Iturbe, I., Porporato, A., Ridolfi, L., Isham, V., Cox, D.R., 1999. Probabilistic modelling of water balance at a point: the role of climate, soil and vegetation. Proc. R. Soc. London, Ser. A 455, 3789–3805.
Sacks, W., Schimel, D.S., Monson, R.K., Braswell, B.H., 2006. Model-data synthesis of diurnal and seasonal CO_2 fluxes at Niwot Ridge, Colorado. Global Change Biol. 12, 240–259.
Sandholt, I., Rasmussen, K., Andersen, J., 2002. A simple interpretation of the surface temperature/vegetation index space for assessment of surface moisture status. Remote Sens. Environ. 79, 213–224.
Schmugge, T., O'Neill, P.E., Wang, J.R., 1986. Passive microwave soil moisture research. IEEE Trans. Geosci. Remote Sens. GE224 (1), 12–211.
Silberstein, R.P., Sivapalan, M., Wyllie, A., 1999. On the validation of a coupled water and energy balance model at small catchment scales. J. Hydrol. 220, 149–168.
Socias, F.X., Correia, M.J., Chaves, M.M., Metrano, H., 1997. The role of abscisic acid and water relations in drought responses of subterranean clover. J. Exp. Bot. 48, 1281–1288.
Topp, G.C., Davis, J.L., Annan, A.P., 1980. Electromagnetic determination of soil water content: measurements in coaxial transmission lines. Water Resour. Res. 16 (3), 574–582.
Walker, B.H., Langridge, J.L., 2006. Modelling plant and soil water dynamics in semi-arid ecosystems with limited site data. Ecol. Model. 87, 153–167.
Weerts, A.H., El Serafy, G.Y.H., 2006. Particle filtering and Ensemble Kalman Filtering for state updating with hydrological conceptual rainfall-runoff models. Water Resour. Res. 42 (9), W09403.
Zhan, Z., Qin, Q., Ghulam, A., Wang, D., 2007. Nir–Red spectral space based new method for soil moisture monitoring. Sci. China, Ser. D 50 (2), 283–289.
Zhang, F., 2004. Impacts of initial estimate and observation availability on convective-scale data assimilation with an Ensemble Kalman Filter. Monthly Weather Rev. 132, 1238–1253.
Zhao, L., Wei, H., Xu, Y., Feng, S., 2005. An adjoint data assimilation approach for estimating parameters in a three-dimensional ecosystem model. Ecol. Model. 186, 234–249.
Zhou, Y., McLaughlin, A., Entekhabi, D., 2006. Assessing the performance of the Ensemble Kalman Filter for land surface data assimilation. Monthly Weather Rev. 134, 2128–2142.